Microporous and Mesoporous Materials 276 (2019) 52–61

Contents lists available at ScienceDirect

Microporous and Mesoporous Materials

journal homepage: www.elsevier.com/locate/micromeso

From amorphous to crystalline: Transformation of silica membranes into silicalite-1 (MFI) zeolite layers

Pelin Karakiliç[a], Ryo Toyoda[a], Freek Kapteijn[b], Arian Nijmeijer[a], Louis Winnubst[a,*]

[a] Inorganic Membranes, MESA+ Institute for Nanotechnology, University of Twente, P.O. Box 217, 7500 AE, Enschede, the Netherlands
[b] Catalysis Engineering, Chemical Engineering Department, Delft University of Technology, Van der Maasweg 9, Delft, Netherlands

ARTICLE INFO

Keywords:
Silicalite-1
MFI zeolite
Silica transformation
Sol-gel
In-situ crystallisation

ABSTRACT

The transformation of microporous, amorphous silica membranes into b-oriented silicalite-1 (MFI) zeolite layers via *in-situ* crystallisation was investigated. The effect of synthesis parameters, such as the type and concentration of the silica precursor, crystallisation time and temperature, on the morphology of silicalite-1 (MFI) zeolite layers was studied. By optimizing these parameters, silicalite-1 zeolite layers were formed from the already-deposited silica layers, which promotes the crystallisation from the surface in the preferred b-orientation. The use of a monomeric silica precursor, which has slower hydrolysis kinetics than a colloidal one, resulted in the formation of zeolite crystals via heterogeneous nucleation on the surface and suppressed the formation of crystal nuclei in the liquid media via homogeneous nucleation, which then would further deposit onto the surface in a random orientation. Lastly, by optimizing the crystallisation time and temperature of the synthesis, thickness, coverage and orientation of silicalite-1 zeolite layers were controlled.

1. Introduction

Zeolites are promising membrane materials for industrial separation applications thanks to their uniform pore size and chemical, thermal and mechanical stability under harsh conditions. In order to maximize the permeance by keeping high separation performance, the zeolite membrane layer should be well-defined in terms of thickness, homogeneity, orientation of the crystals and of a defect-free nature. A myriad of papers have been published about the synthesis and fabrication of zeolite materials, as they are widely used in catalysis [1–5], sensors [6–10], adsorbers [11–13], and in membranes [14–18]. There are 235 zeolite frameworks up to date reported by Structure Commission of the International Zeolite Association (SC-IZA). Among these are the following frameworks reported as zeolite structures used for membrane preparation: AEI [19], BEA [20], CHA [21,22], DDR [23,24], FAU [25,26], FER [27], LTA [28,29], LTL [30], MEL [31], MFI [32–34], MOR [35] and MWW [36]. MFI is the most studied structure due to having micropores which can accommodate and/or separate industrially high-valued molecules. Silicalite-1 is the all-silica zeolite having the MFI framework whereas ZSM-5 is the Al-containing analogue of it.

The channel system of the MFI framework is asymmetric and varies by the orientation of the crystal. The a-orientation (*h*00) has sinusoidal channels, which creates resistance against mass transfer, whereas the b-orientation (0k0) has straight channels, as shown in Fig. 1. The diffusion along these straight channels are three times higher as compared to that along the sinusoidal channels, as reported by Caro et al. [37] and therefore, the b-oriented zeolite layer is preferred to maximise permeance.

The most common method to prepare zeolite membranes is growing zeolite crystals on a porous support. Ways of forming these layers are *in-situ* synthesis and secondary (seeded) growth methods. In the *in-situ* synthesis method, the porous support is placed in a zeolite precursor solution and the zeolite layer is formed via hydrothermal synthesis in an autoclave under autogenous pressure. Here, nucleation and growth of a crystal takes place simultaneously as being a one-step mechanism. On the contrary, the secondary growth method implies separate nucleation and growth steps. In the first step, the nucleation of the crystal occurs in an autoclave in the absence of the porous support, where these seed crystals are recovered from the solution and then deposited on the support. This seed attachment can be done by several methods such as electrophoretic deposition [38,39], dip-coating [40], rubbing [41], pulsed-laser ablation [42] and vacuum seeding [43]. Finally, the seeded support is grown into a continuous layer via a second hydrothermal treatment in the autoclave.

Wang and Yan [44] prepared continuous b-oriented zeolite MFI monolayer films with a thickness of less than 0.4 μm on metal substrates (stainless steel and an aluminium alloy) by *in-situ* crystallisation at

* Corresponding author.
E-mail address: a.j.a.winnubst@utwente.nl (L. Winnubst).

https://doi.org/10.1016/j.micromeso.2018.09.020
Received 29 June 2018; Received in revised form 22 August 2018; Accepted 18 September 2018
Available online 20 September 2018
1387-1811/ © 2018 Elsevier Inc. All rights reserved.

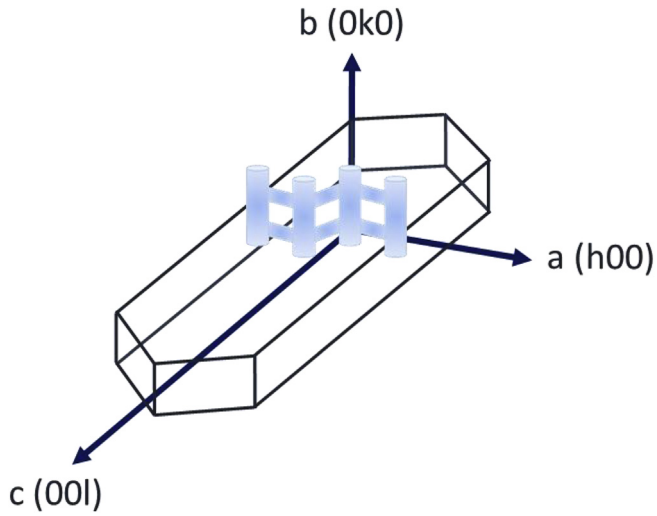

Fig. 1. The channel system along the a- and b-direction of MFI zeolite crystals.

165 °C using a solution with a molar ratio of 1 SiO_2:0.32 TPAOH:165 H_2O where a silica precursor of (monomeric) tetraethyl orthosilicate (TEOS) or colloidal silica (LUDOX-30) was used. They reported that the continuity of the film with b-orientation was provided by using a silica source with a low degree of polymerisation such as TEOS, whereas a colloidal silica source, like LUDOX-30 resulted in the formation of randomly oriented large crystals.

Shan et al. [45] prepared silicalite-1 membranes on porous α-Al_2O_3 hollow fibers by the secondary growth method. They used TEOS as a silica precursor and analysed the effect of the crystallisation time (2–12 h) and the concentration of structure directing agent tetrapropylammonium hydroxide (TPAOH) in the secondary growth solution having a molar ratio of 1 SiO_2: 0.12–0.32 TPAOH: 165 H_2O. They reported that a low concentration of TPAOH resulted in a smoother surface. However extremely low concentrations of the TPAOH template caused poor intergrowth of the crystals and formation of intercrystalline pores because of preferential growth of the seed crystals along the c-axis. In addition, the layer thickness and the zeolite crystal size were increasing after longer crystallisation time, providing continuity of the membrane layer, whereas a short synthesis time resulted in empty spots and gaps.

Mintova and Valtchev [46] investigated the effect of different silica precursors, tetraethyl orthosilicate (TEOS), colloidal silica (LUDOX LS-30) and fumed silica (Cab-O-Sil®), on the synthesis of nanosized silicalite-1 zeolites using a molar composition of 25 SiO_2:9 TPAOH:0.13 Na_2O:420 H_2O:100 EtOH. They reported that the size of the silicalite-1 nanocrystals was 15, 25 and 50 nm using TEOS, Cab-O-Sil and LUDOX AS-30 precursors, respectively, as measured by in-situ dynamic light scattering (DLS) using the backscattering technique. So clearly an influence of precursor used on silicalite-1 crystal size is observed.

Decoupling the nucleation and growth as is the case in the secondary growth method results in a better control of zeolite growth compared with *in-situ* growth. Yet, the optimization of the thickness of the zeolite layer as well as the possibility to obtain an oriented crystal structure by this method are issues still to be tackled for the zeolite membrane fabrication. Hence, it is important to develop new approaches for the fabrication of thin, preferentially-oriented and defect-free zeolite membranes.

Transformation of sol-gel derived amorphous microporous silica layers into zeolite membranes is a recent and novel strategy used for the formation of a zeolite layer. The benefit of this method is that the silica layer can act as a smooth nucleation layer to form all-silica zeolite membranes by *in-situ* zeolite layer formation. As the zeolite crystals are formed from a silica precursor that is already deposited on the surface (i.e. the amorphous silica layer), this method triggers the formation of b-oriented silicalite-1 zeolite crystals. Aguado et al. [47] proved the applicability of using an amorphous microporous silica layer deposited on alumina discs by using colloidal silica as a precursor to prepare b-oriented MFI layers. Moreover, Deng and Pera-Titus [48] used 200 nm thick mesoporous silica coated alumina discs and prepared 500 nm thick b-oriented MFI films. Furthermore, Zhang et al. [49] showed that mesoporous silica coated alumina substrates improved the formation of b-oriented MFI zeolite layers whereas no silica layer coated alumina substrates yielded in random orientation of crystals with poor crystal intergrowth.

Here, in this work, we extend the investigation on transformation of microporous amorphous silica membranes into zeolite layers. By studying several process parameters such as the crystallisation time, crystallisation temperature, concentration and type of silica precursor used during the hydrothermal synthesis, a fundamental understanding was gained on the formation of zeolite layers by transforming an amorphous microporous silica membrane layers.

2. Experimental

The asymmetric silica membranes are prepared by sol-gel chemistry and the final structure is composed of the following three layers: 1) a macroporous, polished and disc-shaped α-Al_2O_3 substrate with 2 mm thickness, 35% porosity and 80 nm pore size were obtained from Pervatech B.V. the Netherlands; 2) a mesoporous γ-Al_2O_3 layer with a pore size of 5 nm and thickness of 3 μm coated on the α-Al_2O_3 disc in order to create an intermediate layer working as a bridge to avoid penetration of the relatively small silica particles into the large pores of the α-Al_2O_3 layer; 3) an amorphous silica top layer with a uniform microstructure having a pore size of much less than 0.5 nm and thickness around 100 nm was coated via sol-gel techniques on the γ-Al_2O_3 intermediate layer [50,51]. The detailed preparation procedure of these silica multilayer membranes is described in Ref. [52].

The sides and bottom of these alumina-supported silica membranes were covered with Teflon tape to make sure that zeolite crystals were only formed via the amorphous silica layer. Then, the surface of the membrane was soaked in a tetrapropylammonium hydroxide (TPAOH, 1.0 M in H_2O, Sigma Aldrich) solution for 2 h prior to the hydrothermal

Table 1
Thickness and crystal orientation of zeolite layers, made by the in-situ synthesis mechanism, using different silica precursors and crystallization time. In all cases the crystallization temperature was 170 °C and the molar composition was 1 Si: 0.05 TPAOH: 0.15 NaOH: 94 H_2O.

Sample No	Precursor	Crystallisation time [h]	Thickness [μm]	Orientation
S1	Colloidal (LUDOX)	17	200	random
S2	Colloidal (LUDOX)	14	147	random
S3	Colloidal (LUDOX)	10	56	random
S4	Colloidal (LUDOX)	4	20	random
S5	Monomeric (TEOS)	10	80	random
S6	Monomeric (TEOS)	7	65	random
S7	Monomeric (TEOS)	4	18	b-oriented[a]

[a] Minor amounts of a-oriented crystals.

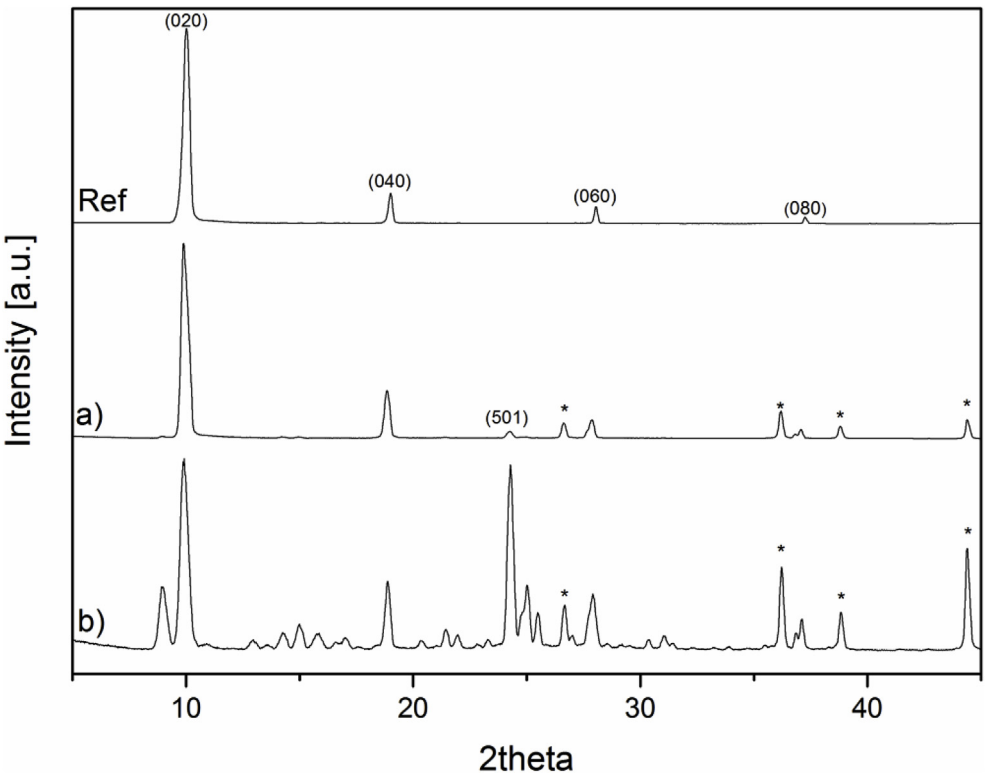

Fig. 2. XRD patterns of layers formed using a) monomeric b) colloidal silica precursor with the same molar ratio in the in-situ synthesis solution of 1 Si: 0.05 TPAOH: 0.15 NaOH: 94 H_2O at 170 °C and for 4 h of synthesis. Ref stands for b-oriented (0k0) crystal peaks of MFI structure obtained from Ref. [53] and asterisk (*) represents the peaks origining from the alumina substrate.

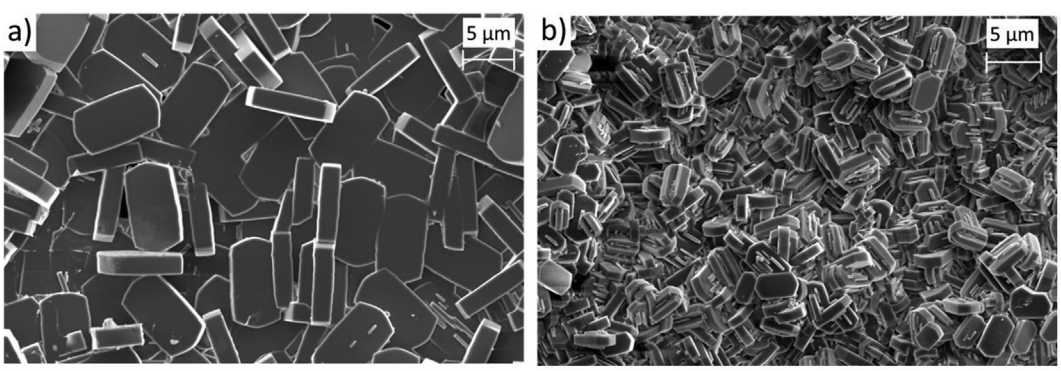

Fig. 3. The surface images of zeolite layers using a) monomeric and b) colloidal silica precursor with the same molar ratio in the in-situ synthesis solution of 1 Si: 0.05 TPAOH: 0.15 NaOH: 94 H_2O and for 4 h of synthesis at 170 °C.

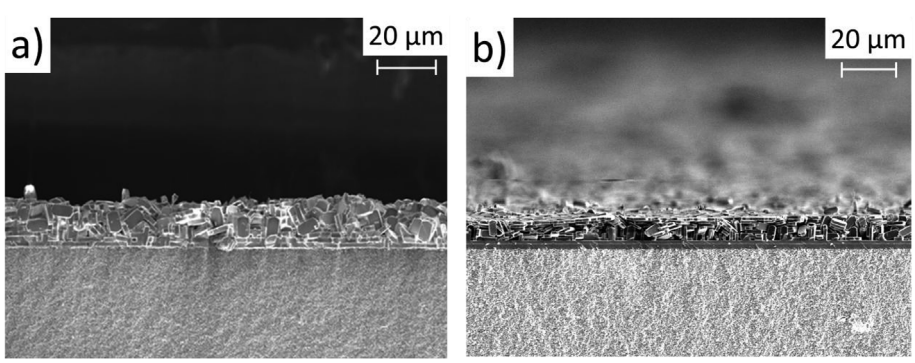

Fig. 4. Cross-sectional SEM images of TEOS-derived silicalite-1 zeolite membrane with different dilution of the precursor solution, a) and b) represent the Si:H_2O ratio of 1:94 and 1:130 respectively, using TEOS silica precursor, at 170 °C and for 4 h of synthesis.

synthesis in order to activate the silicon centres on the amorphous silica network to react them with TPAOH for the further transformation into the zeolite crystals during the hydrothermal treatment. In this way all nutrients required for the zeolite synthesis, being the structure directing agent and the silica source, are available on the membrane surface.

For this *in-situ* zeolite synthesis method two different silica

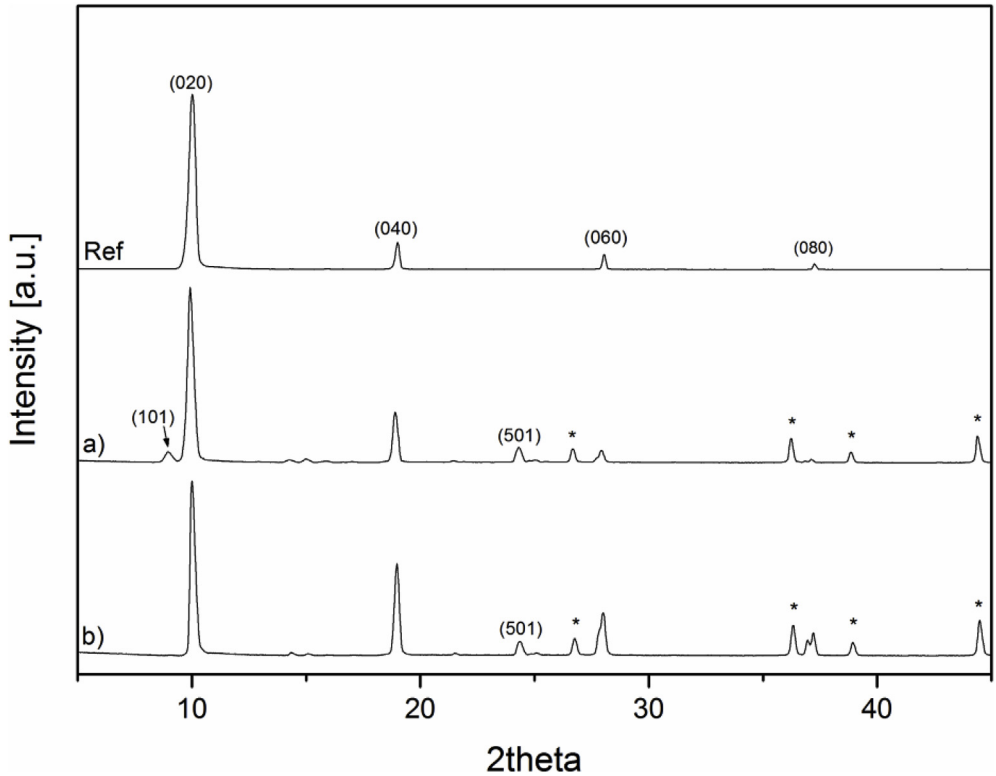

Fig. 5. XRD patterns of layers formed using Si:H_2O ratio of a) 1:94 b) 1:130 using TEOS silica precursor, at 170 °C and for 4 h of synthesis. Ref stands for b-oriented (0k0) crystal peaks of MFI structure obtained from Ref. [53] and asterisk (*) represents the peaks originating from the alumina substrate.

precursors were used: LUDOX® AS-40 colloidal silica (40 wt% suspension in H_2O, Sigma Aldrich) and tetraethyl orthosilicate (TEOS, ≥ 99.0% (GC), Sigma Aldrich) as a monomeric silica. The LUDOX® AS-40 colloidal silica precursor solution was prepared by mixing 7.76 g LUDOX AS-40 with 3.15 g of TPAOH, 0.32 g of sodium hydroxide (NaOH, ACS reagent ≥98% pellets, Sigma Aldrich) and 27.65 g Milli-Q water. In this way a molar ratio was obtained of 1 Si: 0.05 TPAOH: 0.15 NaOH: 37.5 H_2O. The TEOS precursor solution was prepared by mixing 10.8 g of TEOS with 3.15 g of TPAOH, 0.32 g of NaOH and 37.5 g Milli-Q water, resulting in a molar ratio of 1 Si: 0.05 TPAOH: 0.15 NaOH: 37.5 H_2O. So, both precursor solutions have identical concentrations.

In both cases the solution was aged for 1.5 h under vigorous stirring. After that, the solutions were diluted with Milli-Q water to obtain the final molar ratios of 1 Si: 0.05 TPAOH: 0.15 NaOH: 94 H_2O and 1 Si: 0.05 TPAOH: 0.15 NaOH: 130 H_2O, and continued to stir for an additional 30 min. The TPAOH-activated silica membranes were placed horizontally on the bottom of the 125 mL Teflon-lined stainless steel autoclave (Parr Instrument Company) and 70 mL of the solution was added. After sealing, the autoclave was placed into a furnace (FED 56, BINDER) for the hydrothermal synthesis under autogenous pressure. After cooling the autoclave, the membranes were recovered and washed thoroughly with Milli-Q water and dried at 80 °C for 12 h in BINDER FED 56 drying oven.

The surface morphology and thickness (by means of cross sections) of the zeolite layers were determined by JEOL JSM 6010LA scanning electron microscope (SEM) at an accelerating voltage of 5 kV. The SEM was equipped with an energy dispersive X-ray spectrometer (EDX) to have a semi-quantitative elemental analysis of the samples. The surface and cross section of the membrane layers were coated with 5 nm thick Cr which was deposited by sputter coating prior to the analysis.

The XRD patterns are collected by a Bruker D2 Phaser X-ray diffraction with Cu-Kα radiation (λ = 1.5418 nm) in the 2θ range 5–45°, using steps of 0.02°. The peaks were normalized with respect to the highest intensity peak in the 2θ spectrum from 5 to 45°. Then, the crystal structure and orientation of the zeolite layer was analysed by comparing the measured XRD patterns with the reference pattern obtained from the website of the International Zeolite Association [53].

3. Results and discussion

3.1. Zeolite layers using colloidal and monomeric silica precursors at different crystallisation time

In a first series of experiments, the zeolite layers were fabricated by using two different silica precursors: Colloidal silica (LUDOX® AS-40) and monomeric silica (TEOS). The *in-situ* synthesis took place at 170 °C using a molar composition of 1 Si: 0.05 TPAOH: 0.15 NaOH: 94 H_2O for a varying synthesis times as given in Table 1.

The effect of the crystallisation time on the thickness and crystal orientation of the zeolite layer is clearly shown; an increase in crystallisation time results in an increase in layer thickness. In addition to the formation of the crystals on the surface via heterogeneous nucleation, at longer crystallisation time also seed crystals are formed in the solution by homogeneous nucleation and deposited on the surface. Therefore, at longer crystallisation time, due to the random deposition of the crystals formed via homogeneous nucleation in the solution, the zeolite layer was found to be randomly oriented (as determined by XRD).

In addition to the crystallisation time, also the effect of precursor type was studied: colloidal or monomeric. For 4 h of synthesis, even though the thickness of the colloidal silica and monomeric silica derived zeolite layers are similar (20 nm for S4 and 18 μm for S7), the crystal orientation was found to be random when using a colloidal silica precursor. On the other hand, the use of monomeric silica results in b-oriented structure with only minor amounts of a-oriented crystals after 4 h of hydrothermal treatment at 170 °C. This influence of the type of precursor used on crystallographic orientation can be seen from the XRD patterns as given in Fig. 2. By using the monomeric silica, b-

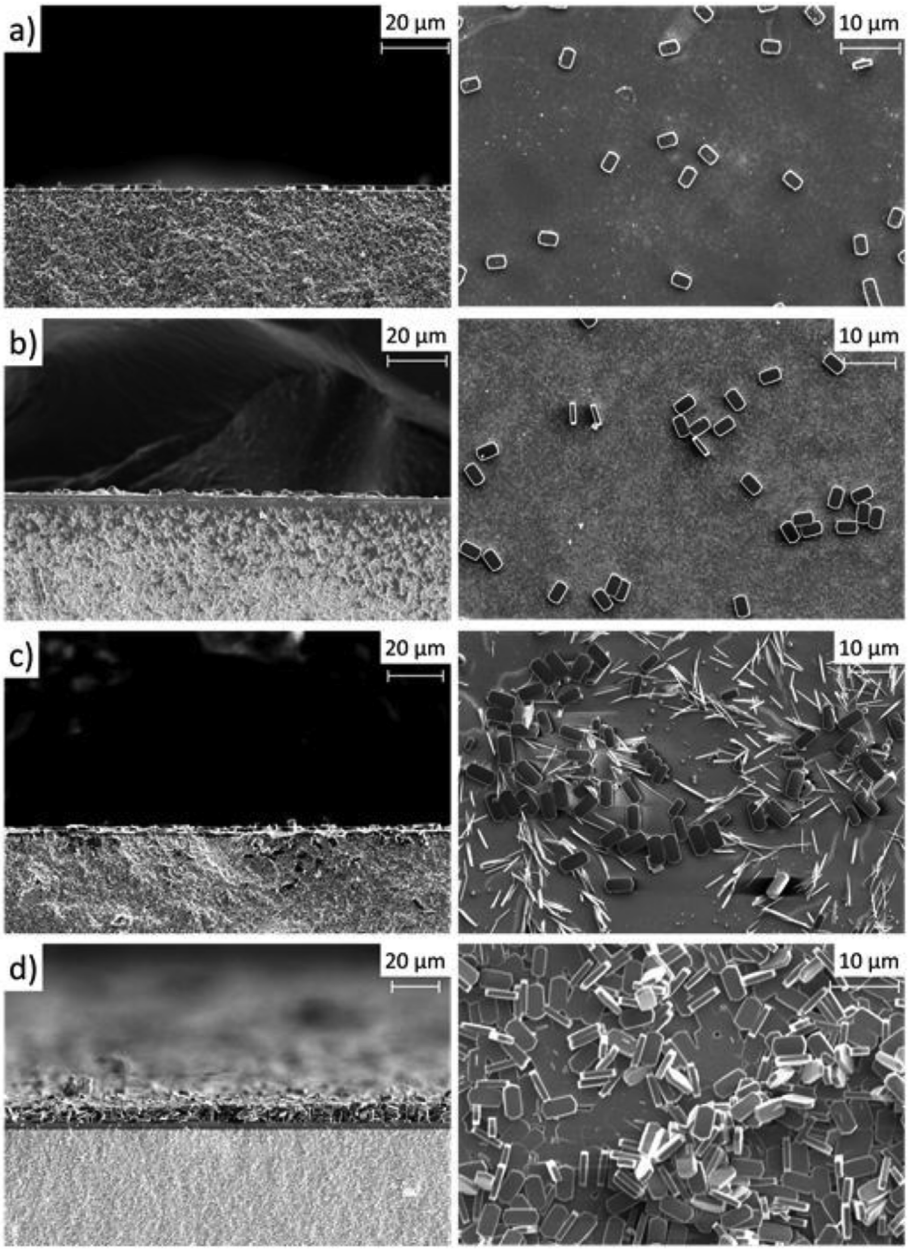

Fig. 6. The cross-sectional (left) and surface images (right) of TEOS derived silicalite-1 layers formed after a) 2 h, b) 3 h, c) 3.5 h and d) 4 h of synthesis at 170 °C.

oriented silicalite-1 layer was formed which has all the reference peaks of (0k0). On the contrary, colloidal silica derived silicalite-1 layer has many other peaks showing the random orientation of the crystals.

Wang and Yan [44] argued that the low degree of condensation in the TEOS precursor favours the formation of oriented layers whereas a colloidal silica precursor results in randomly oriented zeolite layers. This difference can be explained by the fact that crystallisation using a monomeric silica, like TEOS, is three times slower compared to colloidal silica, like LUDOX AS-40 [54]. Therefore, compared to colloidal silica, the formation of nuclei (by homogeneous nucleation) in the liquid phase is suppressed when using a monomeric silica. When colloidal silica is used, deposition of the homogeneously nucleated crystals on the membrane surface results in the formation of an irregular arrangement of zeolite crystals and a relative thick layer on the surface (see Fig. 3b). So, by using monomeric silica mainly heterogeneous nucleation occurs from the already deposited amorphous silica layer. This promotes formation from the surface of a zeolite layer along the b-orientation. This is also visible on the surface images of TEOS and LUDOX derived zeolite layers as given in Fig. 3.

The results, as summarized in Table 1, showed that the layer thickness can be reduced by reducing the synthesis time and that TEOS silica precursor promotes the formation of a b-oriented layer. Therefore, in the next sections only TEOS as precursor is discussed in the search for the most optimal experimental conditions to obtain a thin and b-oriented silicalite-1 layer homogeneously covered on a porous support.

3.2. Influence of Si:H_2O ratio and crystallisation temperature

TEOS as precursor and 4 h of synthesis time were used while studying the effect of the Si concentration in the precursor on silicalite-1 layer formation. Two zeolite layers were prepared using precursor solutions with Si:H_2O ratios of 1:94 and 1:130 respectively. The cross-sectional SEM images of these layers are given in Fig. 4.

The α-alumina support and γ-alumina layer remained intact and are visible in the SEM images. The transformed zeolite layer with lower silica concentration (Si:H_2O of 1:130) showed a thinner layer (8 µm,

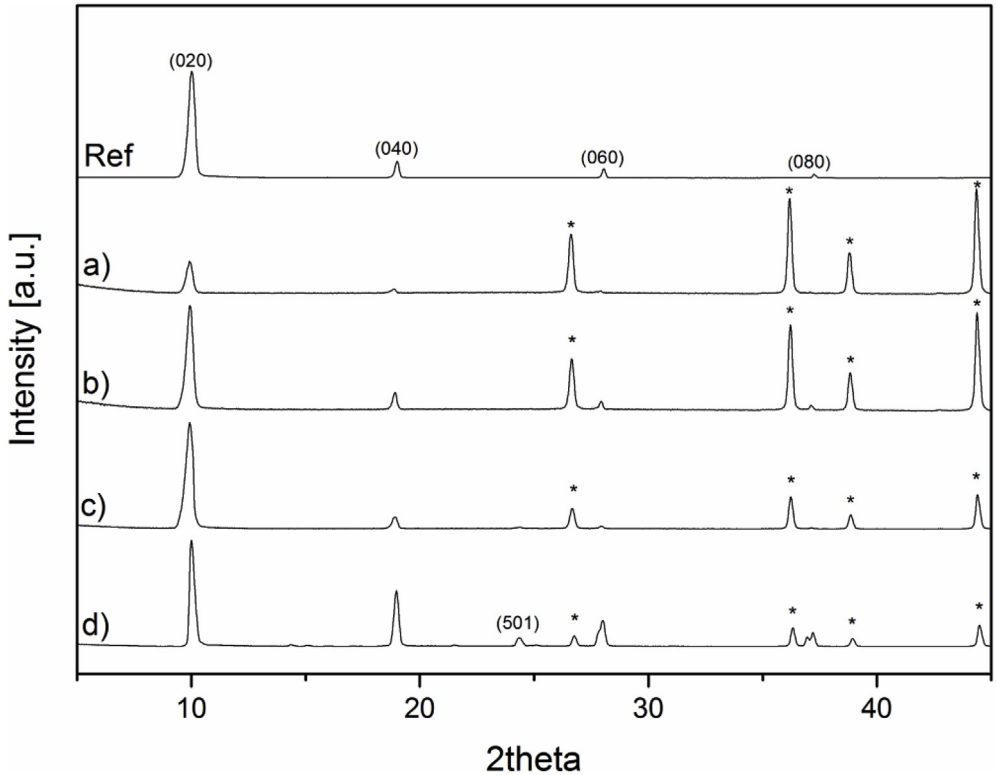

Fig. 7. The XRD pattern of the layers produced for a) 2 h, b) 3 h, c) 3.5 h and d) 4 h of crystallization time. Ref stands for b-oriented (0k0) crystal peaks of MFI structure obtained from Ref. [53] and asterisk (*) represents the XRD signals of the alumina substrate.

Fig. 4b) if compared to the one with the higher silica concentration (Si:H_2O of 1:94, 18 μm, Fig. 4b). Also, the XRD patterns were studied and given in Fig. 5.

XRD results of both zeolite layers were found to have almost similar peaks, as can be seen in Fig. 5. Most of the peaks correspond to the b-orientation (0k0). In addition a small (501) signal was found, while the zeolite layer, made from a precursor with a lower silica concentration (Si:H_2O of 1:130), also showed a peak belonging to (101). Both (501) and (101) signals confirm the presence of a small amount of randomly oriented crystals formed using higher silica concentration.

Based on these results of having thinner layer and less randomly oriented crystals, further studies were done with the lower Si:H_2O ratio of 1:130. In order to investigate at which point the crystallisation starts and the surface is completely covered with b-oriented zeolite crystals, the crystallisation time (at 170 °C) was further decreased from 4 h to 3.5, 3 and 2 h respectively, while keeping TEOS as a silica precursor and the molar ratio of 1 Si:0.05 TPAOH:0.15 NaOH:130 H_2O. The results of these experiments are summarized in Fig. 6. As can be seen form these SEM images a synthesis time shorter than 4 h only results in the formation of a few crystals and not in the formation of a complete zeolite layer on the γ-alumina layer of the support.

The XRD patterns of these layers, formed after different crystallisation times, were given in Fig. 7.

After 2 and 3 h of synthesis the XRD peaks with the highest intensity originate from the Al_2O_3 substrate (Fig. 7a and b). This is due to the incomplete zeolite layer formation. The peaks belonging to the (0k0) b-oriented silicalite-1 structure become more visible when the synthesis time was increased. Only in the layer formed for 4 h of synthesis, all b-orientation peaks were visible in addition to some weak peaks such as (501) due to randomly placement of some crystals as also found in Fig. 6d. After 3.5 h of synthesis time the surface was not completely covered with a zeolite layer (Fig. 6c) So, it was concluded that the 4 h of synthesis is required to form complete and b-oriented zeolite layer while keeping TEOS precursor and the Si:H_2O ratio of 1:130.

3.3. Influence of crystallisation temperature

Finally the crystallisation temperature was varied in order to find the optimal synthesis conditions. The molar composition was kept on 1 Si: 0.05 TPAOH: 0.15 NaOH: 130 H_2O, while TEOS was used as silica precursor and 4 h crystallization time where the crystallisation temperature was varied from 130 to 190 °C. The results of the different surface morphologies as function of crystallisation temperature are summarized in Fig. 8.

It can be clearly seen that 130 °C was far too low for transforming the amorphous silica layer into silicalite-1 crystals and covering the surface completely (Fig. 8a). When temperature was increased to 140 °C, the layer was covered with crystals. Further increase in temperature to 150 °C and 160 °C gave b-oriented monolayer coverage of the crystals on the surface with some visible gaps in between the crystals. At 170 °C, the complete coverage of b-oriented zeolite was visible on the membrane surface together with some loosely bound secondary crystals on the surface as seen in Fig. 8e. These latter crystals were presumably formed by homogeneous nucleation of zeolite crystals from the solutions and subsequently deposited on the surface. When the crystallisation temperature increased even further to 180 and 190 °C, the crystals grew too rapidly and deposited randomly on the surface as also observed in other work [44,55].

The XRD pattern of the layers formed at different crystallisation temperatures are provided in Fig. 9.

The intensity of the (0k0) peaks (ascribed to b-orientation) from the layers at lower temperatures (130 °C and 140 °C) were too low and insignificant as compared to the peaks coming from the alumina support due to uncomplete coverage of the zeolite layer, which was also clearly seen in Fig. 8. The peaks, corresponding to the b-orientation, were all visible in the samples synthesized at 150 °C, 160 °C and 170 °C. The layers prepared at 180 and 190 °C consist of randomly oriented crystals as observed by XRD by having many peaks other than those belonging to b-orientation. This more random orientation of the crystals

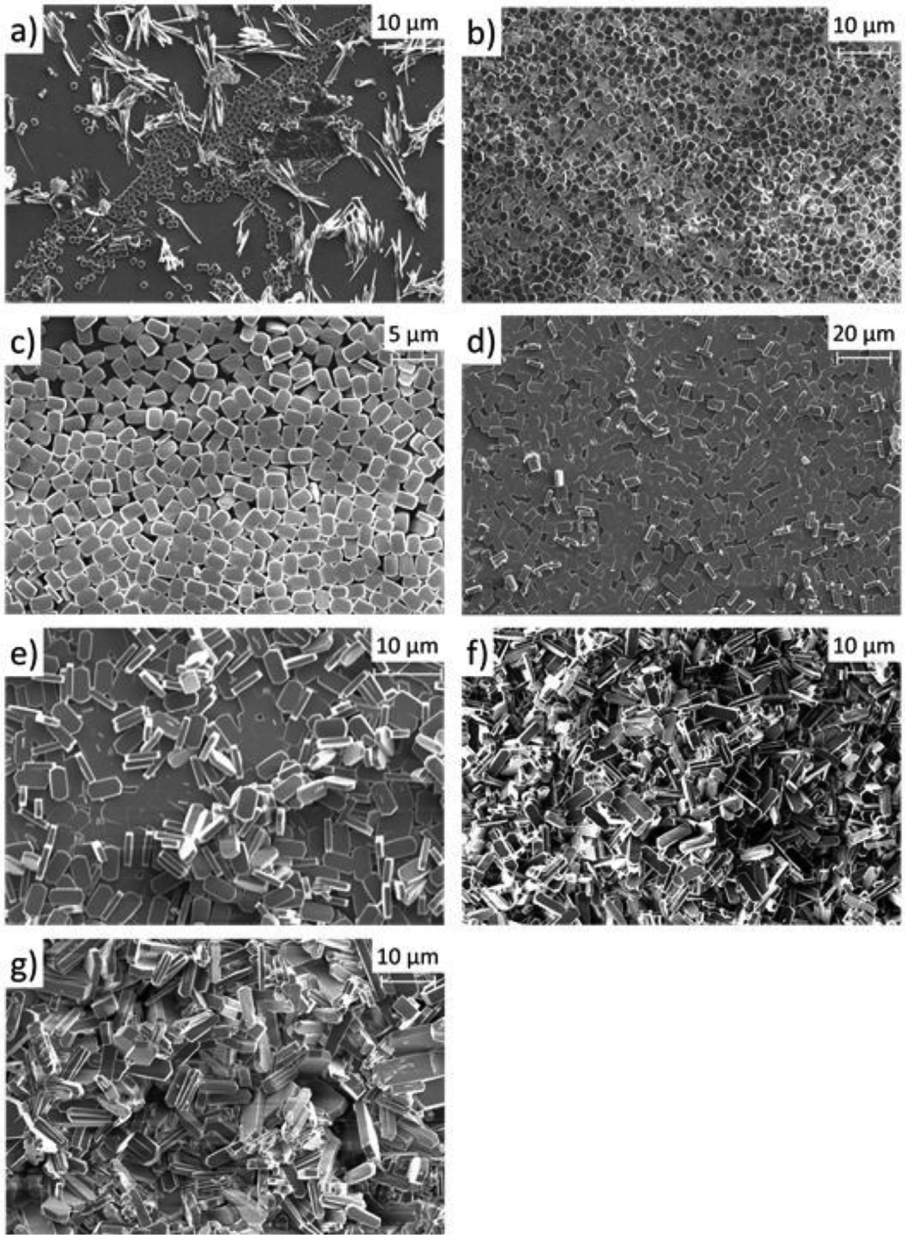

Fig. 8. The effect of synthesis temperature on the size of crystals and surface coverage of the zeolite layer where letters represent the synthesis temperature: a) 130 °C, b) 140 °C, c) 150 °C, d) 160 °C, e) 170 °C, f) 180 °C and g) 190 °C.

is also clearly shown in the SEM images in Fig. 8f and g if compared with e.g. Fig. 8e. Also, the lower signal from the substrate as compared to the zeolite layer peaks is clearly observed in these two layers which is due to very thick layer formation consisting of large crystals. Furthermore, at these high temperatures the crystals were randomly oriented due to the rapid growth and random deposition of the crystals.

All these results indicate the following optimal synthesis parameters when using the novel synthesis method of the transformation an amorphous and microporous silica layer to a b-oriented silicalite-1 layer: Using TEOS silica precursor in the in-situ synthesis solution with a molar composition of 1 Si:0.05 TPAOH:0.15 NaOH:130 H_2O and perform the crystallization reaction in an autoclave for 4 h at temperatures varying from 150 to 170 °C to fabricate a thin and b-oriented silicalite-1 zeolite layer with complete surface coverage.

3.4. Elemental analysis on the in-situ transformed silicalite-1 layers

In order to confirm the all-silica nature of the silicalite-1 layer without any incorporation of aluminium that would possibly leach from the alumina substrate, SEM/EDX analyses were done on a cross section, which image is given in Fig. 10. This is a SEM picture of a sample, made by one of the optimal synthesis conditions; i.e. TEOS precursor, 4 h of crystallisation at 150 °C. Form this figure it can also be seen that the γ-alumina layer preserves its initial thickness of 3 µm after the hydrothermal synthesis, while the zeolite crystals are nicely oriented in the b-direction perpendicular to the surface (compare with Fig. 1). The letters in the image represent the spots where the elemental analyses were performed and the results on Al, Si and O elemental composition are tabulated in Table 2. The zeolite layer (points A and B in Fig. 10) was found to be Al-free, proving that it is an all-silica silicalite-1 (MFI) layer. In addition, the Al:O atomic ratios of around 1:1.5 of the γ-Al2O3 (point C) and α-Al2O3 (point D) layers indicate no elemental change on the

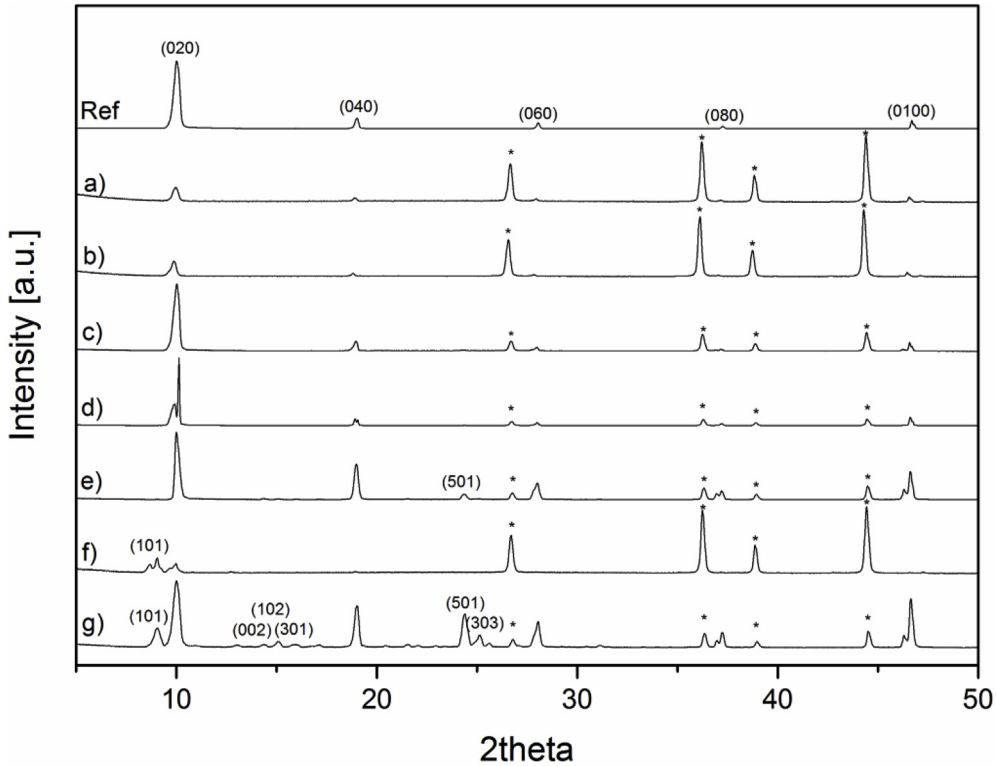

Fig. 9. The powder pattern of the layers formed at a) 130 °C, b) 140 °C, c) 150 °C, d) 160 °C, e) 170 °C, f) 180 °C and g) 190 °C. Ref stands for b-oriented (0k0) crystal peaks of MFI structure obtained from Ref. [53] and asterisk (*) represents the peaks coming from the alumina substrate.

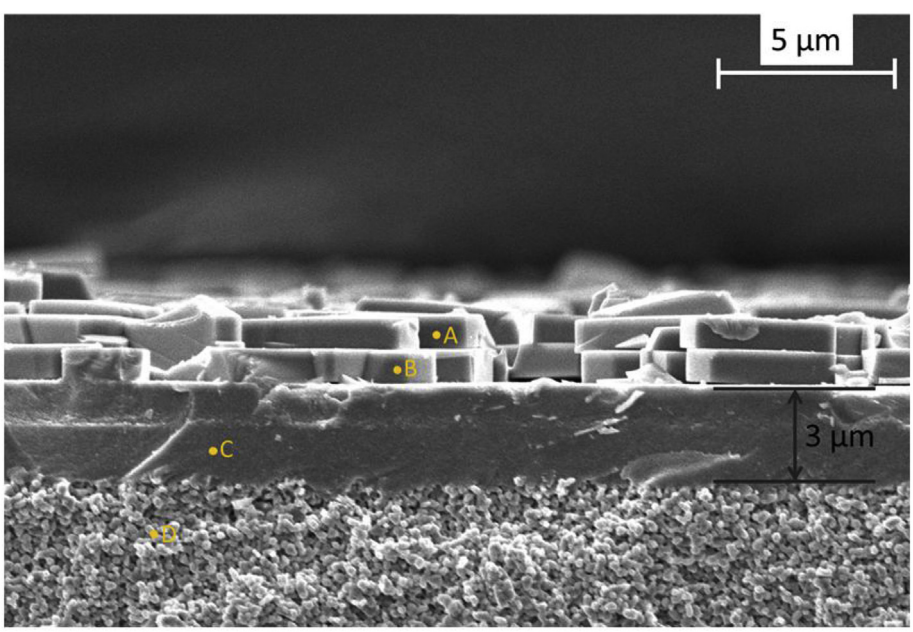

Fig. 10. SEM image of the in-situ synthesized silicalite-1 layers using TEOS precursor, 4 h of crystallisation and 150 °C of synthesis temperature. The letters A, B, C and D correspond to the regions analysed by EDX, to determine the elemental composition.

Table 2
Elemental EDX analysis results from SEM image in Fig. 10.

Position	Si [atom%]	Al [atom%]	O [atom%]
A	32	0	68
B	31	0	69
C	0	29	71
D	0	39	61

substrate.

4. Conclusions

In this work an optimal route is developed for the synthesis of a b-oriented silicalie-1 layer by starting from an amorphous, microporous, silica layer as applied on an α-alumina supported γ-alumina membrane. The synthesis parameters studied were the type and concentration of

silica precursor, the hydrothermal crystallization time and temperature. By optimizing all these parameters, a thin layer and complete coverage of a b-oriented silicalite-1 layer was obtained and a better understanding was achieved on how a pre-deposited silica layer transformed under specific synthesis parameters. These optimal conditions are the use of a monomeric (TEOS) silica precursor instead of colloidal silica (LUDOX® AS-40) and a molar composition of 1 Si:0.05 TPAOH:0.15 NaOH:130 H2O, while performing the crystallization reaction in an autoclave for 4 h at temperatures varying from 150 to 170 °C. EDX analysis showed that no aluminium leaching from the α/γ-alumina support to the zeolite layer was found during the *in-situ* transformation, indicating that all-silica zeolite layers are formed.

Further research could be dedicated to applying post-treatment methods for healing any defects or pinholes between these zeolite crystals in order to take advantage of these preferably-oriented layers for use as a membrane material for gas and liquid separation, having high fluxes provided by its b-oriented channels.

Acknowledgment

This research is supported by Netherlands Technology Foundation (STW-13941). The authors acknowledge Cindy Huiskes and Mieke Luiten-Olieman from University of Twente, and Xuerui Wang from Delft University of Technology for their helpful discussions in this work and Frank Morssinkhof from University of Twente for technical support. The authors declare no conflict of interest.

References

[1] X. Lu, Y. Peng, Z. Wang, Y. Yan, Rapid fabrication of highly b-oriented zeolite MFI thin films using ammonium salts as crystallization-mediating agents, Chem. Commun. 51 (2015) 11076–11079, https://doi.org/10.1039/C5CC02980E.
[2] M.S. Holm, E. Taarning, K. Egeblad, C.H. Christensen, Catalysis with hierarchical zeolites, Catal. Today 168 (2011) 3–16, https://doi.org/10.1016/j.cattod.2011.01.007.
[3] J. Weitkamp, Zeolites and catalysis, Solid State Ionics 131 (2000) 175–188, https://doi.org/10.1016/S0167-2738(00)00632-9.
[4] D. Fu, J.E. Schmidt, Z. Ristanović, A.D. Chowdhury, F. Meirer, B.M. Weckhuysen, Highly oriented growth of catalytically active zeolite ZSM-5 films with a broad range of Si/Al ratios, Angew. Chem. Int. Ed. 56 (2017) 11217–11221, https://doi.org/10.1002/anie.201704846.
[5] I. Yarulina, A. Dikhtiarenko, F. Kapteijn, J. Gascon, Consequences of secondary zeolite growth on catalytic performance in DMTO studied over DDR and CHA †, Catal. Sci. Technol. 7 (2017) 300–309, https://doi.org/10.1039/C6CY02307J.
[6] W.L. Rauch, M. Liu, Development of a selective gas sensor utilizing a perm-selective zeolite membrane, J. Mater. Sci. 38 (2003) 4307–4317, https://doi.org/10.1023/A:1026331015093.
[7] P. Yang, X. Ye, C. Lau, Z. Li, X. Liu, J. Lu, Design of efficient zeolite sensor materials for n-hexane, Anal. Chem. 79 (2007) 1425–1432, https://doi.org/10.1021/ac061811+.
[8] A. Satsuma, D. Yang, K. Shimizu, Effect of acidity and pore diameter of zeolites on detection of base molecules by zeolite thick film sensor, Microporous Mesoporous Mater. 141 (2011) 20–25, https://doi.org/10.1016/j.micromeso.2009.12.002.
[9] X. Xu, J. Wang, Y. Long, Zeolite-based materials for gas sensors, Sensors 6 (2006) 1751–1764, https://doi.org/10.3390/s6121751.
[10] S. Mintova, S. Mo, T. Bein, Humidity sensing with ultrathin LTA-type molecular sieve films grown on piezoelectric devices, Chem. Mater. 13 (2001) 901–905, https://doi.org/10.1021/cm000671w.
[11] R.V. Siriwardane, M.S. Shen, E.P. Fisher, J. Losch, Adsorption of CO_2 on zeolites at moderate temperatures, Energy Fuels 19 (2005) 1153–1159, https://doi.org/10.1021/ef040059h.
[12] S.M. Kuznicki, V.A. Bell, S. Nair, H.W. Hillhouse, R.M. Jacubinas, C.M. Braunbarth, et al., A titanosilicate molecular sieve with adjustable pores for size-selective adsorption of molecules, Nature 412 (2001) 720–724, https://doi.org/10.1038/35089052.
[13] S. Velu, X. Ma, C. Song, Selective adsorption for removing sulfur from jet fuel over zeolite-based adsorbents, Ind. Eng. Chem. Res. 42 (2003) 5293–5304, https://doi.org/10.1021/ie020995p.
[14] J.L. Hang Chau, C. Tellez, K.L. Yeung, K. Ho, The role of surface chemistry in zeolite membrane formation, J. Membr. Sci. 164 (2000) 257–275, https://doi.org/10.1016/S0376-7388(99)00214-8.
[15] N. Kosinov, C. Auffret, C. Gücüyener, B.M. Szyja, J. Gascon, F. Kapteijn, et al., High flux high-silica SSZ-13 membrane for CO_2 separation, J. Mater. Chem. A. 2 (2014) 13083–13092, https://doi.org/10.1039/C4TA02744B.
[16] L. Sandström, E. Sjöberg, J. Hedlund, Very high flux MFI membrane for CO_2 separation, J. Membr. Sci. 380 (2011) 232–240, https://doi.org/10.1016/j.memsci.2011.07.011.
[17] J. Jiang, L. Wang, L. Peng, C. Cai, C. Zhang, X. Wang, et al., Preparation and characterization of high performance CHA zeolite membranes from clear solution, J. Membr. Sci. 527 (2017) 51–59, https://doi.org/10.1016/j.memsci.2017.01.005.
[18] Y. Hasegawa, T. Ikeda, T. Nagase, Y. Kiyozumi, T. Hanaoka, F. Mizukami, Preparation and characterization of silicalite-1 membranes prepared by secondary growth of seeds with different crystal sizes, J. Membr. Sci. 280 (2006) 397–405, https://doi.org/10.1016/j.memsci.2006.01.044.
[19] T. Wu, B. Wang, Z. Lu, R. Zhou, X. Chen, Alumina-supported AlPO-18 membranes for CO_2/CH_4 separation, J. Membr. Sci. 471 (2014) 338–346, https://doi.org/10.1016/j.memsci.2014.08.035.
[20] T.C.T. Pham, H.S. Kim, K.B. Yoon, Growth of uniformly oriented silica MFI and BEA zeolite films on substrates, Science 334 (2011) 1533–1538, https://doi.org/10.1126/science.1212472.
[21] H. Kalipcilar, S.K. Gade, R.D. Noble, J.L. Falconer, Synthesis and separation properties of B-ZSM-5 zeolite membranes on monolith supports, J. Membr. Sci. 210 (2002) 113–127, https://doi.org/10.1016/S0376-7388(02)00380-0.
[22] K. Kida, Y. Maeta, K. Yogo, Preparation and gas permeation properties on pure silica CHA-type zeolite membranes, J. Membr. Sci. 522 (2017) 363–370, https://doi.org/10.1016/j.memsci.2016.09.002.
[23] S. Yang, Z. Cao, A. Arvanitis, X. Sun, Z. Xu, J. Dong, DDR-type zeolite membrane synthesis, modification and gas permeation studies, J. Membr. Sci. 505 (2016) 194–204, https://doi.org/10.1016/j.memsci.2016.01.043.
[24] C. Gücüyener, J. van den Bergh, A.M. Joaristi, P.C.M.M. Magusin, E.J.M. Hensen, J. Gascon, et al., Facile synthesis of the DD3R zeolite: performance in the adsorptive separation of buta-1,3-diene and but-2-ene isomers, J. Mater. Chem. 21 (2011) 18386–18397, https://doi.org/10.1039/c1jm13671b.
[25] L. Sandström, J. Lindmark, J. Hedlund, Separation of methanol and ethanol from synthesis gas using MFI membranes, J. Membr. Sci. 360 (2010) 265–275, https://doi.org/10.1016/j.memsci.2010.05.022.
[26] T.F. Mastropietro, E. Drioli, S. Candamano, T. Poerio, Crystallization and assembling of FAU nanozeolites on porous ceramic supports for zeolite membrane synthesis, Microporous Mesoporous Mater. 228 (2016) 141–146, https://doi.org/10.1016/j.micromeso.2016.03.037.
[27] N. Nishiyama, T. Matsufuji, K. Ueyama, M. Matsukata, FER membrane synthesized by a vapor-phase transport method: its structure and separation characteristics, Microporous Mater. 12 (1997) 293–303, https://doi.org/10.1016/S0927-6513(97)00076-X.
[28] A. Huang, F. Liang, F. Steinbach, J. Caro, Preparation and separation properties of LTA membranes by using 3-aminopropyltriethoxysilane as covalent linker, J. Membr. Sci. 350 (2010) 5–9, https://doi.org/10.1016/j.memsci.2009.12.029.
[29] I. Tiscornia, S. Valencia, A. Corma, C. Téllez, J. Coronas, J. Santamaría, Preparation of ITQ-29 (Al-free zeolite A) membranes, Microporous Mesoporous Mater. 110 (2008) 303–309, https://doi.org/10.1016/j.micromeso.2007.06.019.
[30] F. Ghoroghchian, H. Aghabozorg, F. Farhadi, H. Kazemian, Controlled synthesis of a thin LTL zeolitic membrane using nano-sized seeds: characterization and permeation performance, Chem. Eng. Technol. 33 (2010) 2066–2072, https://doi.org/10.1002/ceat.200900543.
[31] N. Kosinov, E.J.M. Hensen, Synthesis and separation properties of an α-alumina-supported high-silica MEL membrane, J. Membr. Sci. 447 (2013) 12–18, https://doi.org/10.1016/j.memsci.2013.07.028.
[32] Z.A.E.P. Vroon, K. Keizer, A.J. Burggraaf, H. Verweij, Preparation and characterization of thin zeolite MFI membranes on porous supports, J. Membr. Sci. 144 (1998) 65–76, https://doi.org/10.1016/S0376-7388(98)00035-0.
[33] M. Zhou, D. Korelskiy, P. Ye, M. Grahn, J. Hedlund, A uniformly oriented MFI membrane for improved CO_2 separation, Angew. Chem. Int. Ed. 53 (2014) 3492–3495, https://doi.org/10.1002/anie.201311324.
[34] M.Y. Jeon, D. Kim, P. Kumar, P.S. Lee, N. Rangnekar, P. Bai, et al., Ultra-selective high-flux membranes from directly synthesized zeolite nanosheets, Nature 543 (2017) 690–694, https://doi.org/10.1038/nature21421.
[35] A. Tavolaro, A. Julbe, C. Guizard, A. Basile, L. Cot, E. Drioli, Synthesis and characterization of a mordenite membrane on an α-Al_2O_3 tubular support, J. Mater. Chem. 10 (2000) 1131–1137, https://doi.org/10.1039/b000047g.
[36] K. Makita, Y. Hirota, Y. Egashira, K. Yoshida, Y. Sasaki, N. Nishiyama, Synthesis of MCM-22 zeolite membranes and vapor permeation of water/acetic acid mixtures, J. Membr. Sci. 372 (2011) 269–276, https://doi.org/10.1016/j.memsci.2011.02.007.
[37] J. Caro, M. Noack, J. Richter-Mendau, F. Marlow, D. Petersohn, M. Griepentrog, et al., Selective sorption uptake kinetics of n-hexane on ZSM-5. A new method for measuring anisotropic diffusivities, J. Phys. Chem. 97 (1993) 13685–13690, https://doi.org/10.1021/j100153a043.
[38] M. Abdollahi, S.N. Ashrafizadeh, A. Malekpour, Preparation of zeolite ZSM-5 membrane by electrophoretic deposition method, Microporous Mesoporous Mater. 106 (2007) 192–200, https://doi.org/10.1016/j.micromeso.2007.02.051.
[39] T. Seike, M. Matsuda, M. Miyake, Preparation of FAU type zeolite membranes by electrophoretic deposition and their separation properties, J. Mater. Chem. 12 (2002) 366–368, https://doi.org/10.1039/b106774p.
[40] X. Wang, Z. Yang, C. Yu, L. Yin, C. Zhang, X. Gu, Preparation of T-type zeolite membranes using a dip-coating seeding suspension containing colloidal SiO_2, Microporous Mesoporous Mater. 197 (2014) 17–25, https://doi.org/10.1016/j.micromeso.2014.05.046.
[41] T.C.T. Pham, T.H. Nguyen, K.B. Yoon, Gel-free secondary growth of uniformly oriented silica MFI zeolite films and application for xylene separation, Angew. Chem. Int. Ed. 52 (2013) 8693–8698, https://doi.org/10.1002/anie.201301766.
[42] D. Coutinho, K.J. Balkus, Preparation and characterization of zeolite X membranes via pulsed-laser deposition, Microporous Mesoporous Mater. 52 (2002) 79–91, https://doi.org/10.1016/S1387-1811(02)00273-1.
[43] A. Huang, Y.S. Lin, W. Yang, Synthesis and properties of A-type zeolite membranes

by secondary growth method with vacuum seeding, J. Membr. Sci. 245 (2004) 41–51, https://doi.org/10.1016/j.memsci.2004.08.001.
[44] Z. Wang, Y. Yan, Oriented zeolite MFI monolayer films on metal substrates by in situ crystallization, Microporous Mesoporous Mater. 48 (2001) 229–238, https://doi.org/10.1016/S1387-1811(01)00357-2.
[45] L. Shan, J. Shao, Z. Wang, Y. Yan, Preparation of zeolite MFI membranes on alumina hollow fibers with high flux for pervaporation, J. Membr. Sci. 378 (2011) 319–329, https://doi.org/10.1016/j.memsci.2011.05.011.
[46] S. Mintova, V. Valtchev, Effect of the silica source on the formation of nanosized silicalite-1: an in situ dynamic light scattering study, Microporous Mesoporous Mater. 55 (2002) 171–179, https://doi.org/10.1016/S1387-1811(02)00401-8.
[47] S. Aguado, E.E. McLeary, A. Nijmeijer, M. Luiten, J.C. Jansen, F. Kapteijn, b-Oriented MFI membranes prepared from porous silica coatings, Microporous Mesoporous Mater. 120 (2009) 165–169, https://doi.org/10.1016/j.micromeso.2008.08.059.
[48] Z. Deng, M. Pera-Titus, In situ crystallization of b-oriented MFI films on plane and curved substrates coated with a mesoporous silica layer, Mater. Res. Bull. 48 (2013) 1874–1880, https://doi.org/10.1016/j.materresbull.2013.01.020.
[49] F. Zhang, M. Fuji, M. Takahashi, In situ growth of continuous b-oriented MFI zeolite membranes on porous α-alumina substrates precoated with a mesoporous silica sublayer, Chem. Mater. 17 (2005) 1167–1173, https://doi.org/10.1021/cm048644j.
[50] R.M. de Vos, H. Verweij, High-selectivity, high-flux silica membranes for gas separation, Science 279 (1998) 1710–1711.
[51] M. ten Hove, M.W.J. Luiten-Olieman, C. Huiskes, A. Nijmeijer, L. Winnubst, Hydrothermal stability of silica, hybrid silica and Zr-doped hybrid silica membranes, Separ. Purif. Technol. 189 (2017) 48–53, https://doi.org/10.1016/j.seppur.2017.07.045.
[52] P. Karakiliç, C. Huiskes, M.W.J. Luiten-Olieman, A. Nijmeijer, L. Winnubst, Sol-gel processed magnesium-doped silica membranes with improved H_2/CO_2 separation, J. Membr. Sci. 543 (2017) 195–201, https://doi.org/10.1016/j.memsci.2017.08.055.
[53] Database of zeolite structures, (n.d.). http://www.iza-structure.org/databases/ (accessed April 27, 2018).
[54] M.D. Oleksiak, J.A. Soltis, M.T. Conato, R.L. Penn, J.D. Rimer, Nucleation of FAU and LTA zeolites from heterogeneous aluminosilicate precursors, Chem. Mater. 28 (2016) 4906–4916, https://doi.org/10.1021/acs.chemmater.6b01000.
[55] A.E. Persson, B.J. Schoeman, J. Sterte, J.-E. Otterstedt, The synthesis of discrete colloidal particles of TPA-silicalite-1, Zeolites 14 (1994) 557–567, https://doi.org/10.1016/0144-2449(94)90191-0.